Plasmonic metasurface-enabled differential photodetectors for broadband optical polarization characterization

Evgeniy Panchenko,* Jasper J. Cadusch, Timothy D. James, and Ann Roberts

School of Physics, University of Melbourne, Victoria 3010, Australia

E-mail: epanchenko@student.unimelb.edu.au

Abstract

The polarization state of an optical field is central to applications in optical communications, imaging and data storage as well as furthering our understanding of biological and physical systems. Here we demonstrate two silicon photodetectors integrated with aluminum nanoantennas capable of distinguishing orthogonal states of either linearly or circularly polarised light with no additional filters. The localised plasmon resonances of the antennas lead to selective screening of the underlying silicon from light with a particular polarization state. The planar device, fully compatible with conventional CMOS fabrication methods, incorporates antennas sensitive to orthogonal states of polarization into two back-to-back Schottky photodetectors to produce a differential electrical signal that changes sign as the polarization of an incident optical beam changes from one basis state to the orthogonal state. The non-null response of the devices to each of the basis states expands the potential utility of the photodetectors while improving precision. Each device is wrapped into a spiral footprint to provide compatibility with the circular profile of conventional optical beams and has an overall diameter of 50 µm. The sensitivity of these devices is demonstrated experimentally

over a wavelength range from 500 to 800 nm establishing their potential for integration into a wide range of optical systems.

Keywords

Photonics, CMOS, Schottky, Diode, Noise suppression, Balanced detector, MSM

Polarization is a fundamental property of electromagnetic radiation that can be used to probe biological[1] and physical[2] systems, as a channel for data transport and storage and as basis states in quantum computing.[3] Polarized light microscopy can elucidate information about orientational order within cells below the diffraction limit[4] or strain and variations in crystal geometry in materials. The use of different polarization states can be used to increase the storage capacity in optical data storage systems[5,6] and the potential for using polarization to increase the bit rate and data security in optical telecommunication systems[7–9] is well-known. Conventional detectors, however, are sensitive to only the intensity of an electromagnetic wave and additional optical elements such as waveplates, polarizers and liquid crystal devices are required in the beam path to determine the state of polarization of the field. Such components are bulky and can compromise the speed and cost of optical systems and limiting their utility.

In response, there has been a significant investment of effort into the miniaturization of optical elements including lenses,[10,11] waveplates[12,13] and polarization filters[14] using plasmonics relying on the excitation of propagating or standing waves on the boundary between a dielectric and a metallic particle or surface. This effort has largely centred on passive optical devices due to the relative ease of fabrication and characterization compared to active optical devices. Recently, however, novel plasmonic nanoantennas have been used in conjunction with Schottky and PIN photodetectors.[15–18] The role of the nanoantennas in these cases include increasing sensitivity,[17] the broadening of the operating range via hot electron injection[16] or polarization selectivity.[15] Polarization sensitive photodiodes found in

the literature tend to respond directly to only one polarization state and have a null or suppressed response to the other. The device demonstrated in,[15] for example, generates a measurable photocurrent for only one of the circular polarization states.

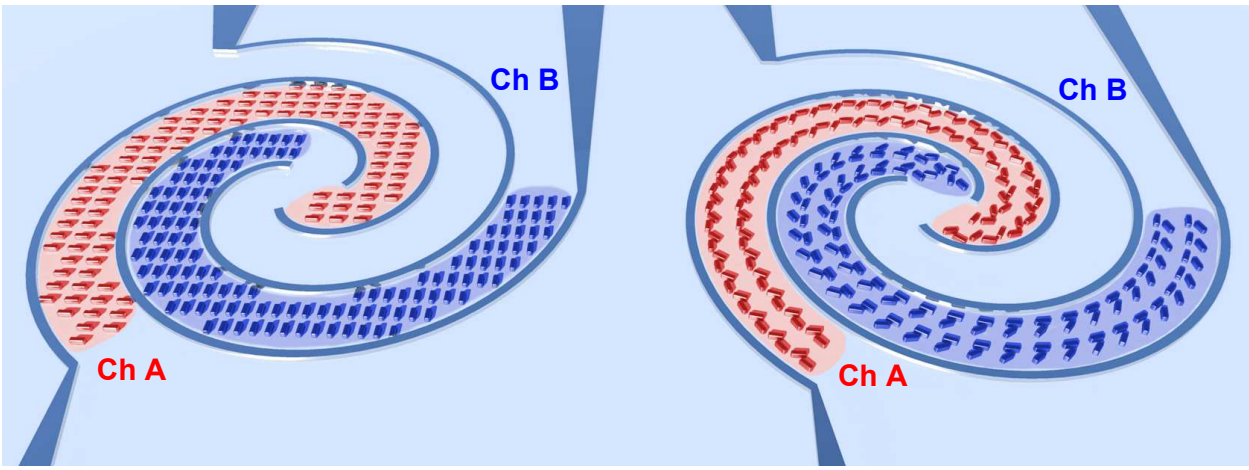

Figure 1: Schematic representation of two spiral MSM photodetectors with rectangular **(left)** and chiral **(right)** nanoantennas.

Here we propose and experimentally demonstrate intregated devices using planar metal-semiconductor-metal (MSM) photodiodes incorporating tailored arrays of plasmonic nanoantennas in the active region of each photodetector that are capable of discriminating between optical signals with different polarizations. The device utilizes a differential detection technique[19–22] which has been shown to significantly improve the robustness of physical systems to noise. The technique involves using two complementary signals and creating a differential response in the detector rather than relying on independent outputs. Therefore, the detector generates a null response only for unpolarized light. The use of aluminum provides broadband performance across much of the visible spectrum. In this paper we fabricated two photodetectors incorporating nanoantennas with a tailored sensitivity to different polarization states. We experimentally demonstrated the ability of each detector to distinguish between either linear or circular polarisations of incident light. The devices are fully compatible with standard CMOS fabrication techniques and the approach presented here could be extended to the extraction of more comprehensive polarization information from an op-

tical field in the form of Stokes parameters as well as exotic polarisation states (for example azimuthal or radial polarization) or different properties such as wavelength or phase. As a consequence, the work presented here demonstrates the potential for a new generation of compact, low-cost detectors which could be used in future optical systems.

Design

Utilization of plasmonic nanoantennas - the analogue of conventional antennas for optical frequencies - permits the creation of metasurfaces sensitive to particular polarization states of light. The electromagnetic properties of such surfaces can be tailored by varying the geometry and constituent materials.[23] Most metasurfaces that consist of nanoantennas with a broken symmetry are intrinsically sensitive to the state of linear polarization of an electromagnetic wave. The simplest and the most widely used antenna shape is the rod which behaves as an electric dipole. Such a geometry has two lower order plasmonic resonances (with dipole moments directed along the short and long axis) that depend on its longitudinal and transverse dimensions. Creating a composite antenna consisting of two appropriately located and oriented nanorods can create an antenna sensitive to other polarization states such as left and right circular polarization.[24] When a metasurface with these properties is placed in front of an active region of photodetector it behaves as a polarization sensitive filter making this detector sensitive to one of the polarization states.

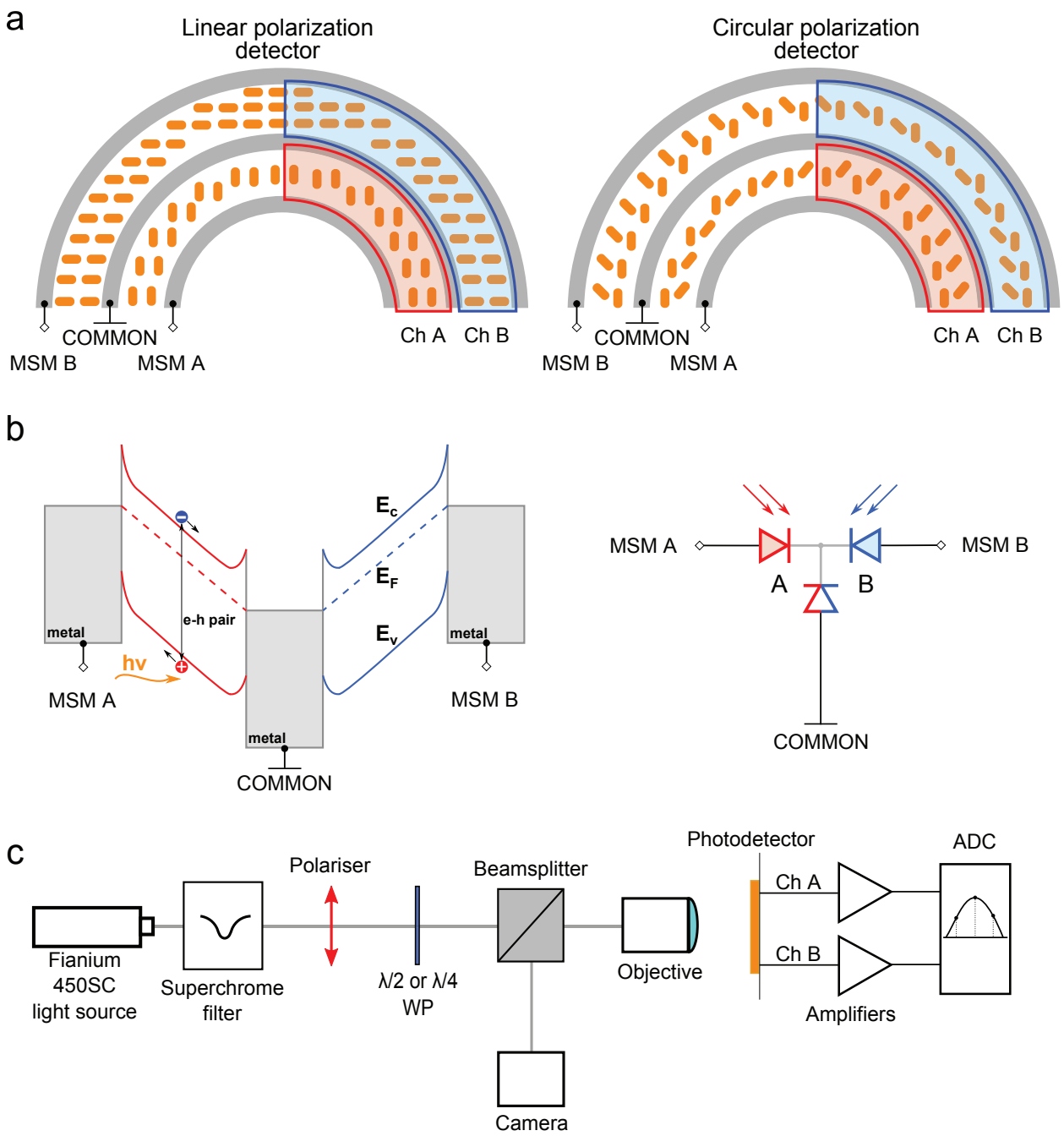

Figure 2: Schematic representation showing both channels of photodetectors integrated with nanorods to sense either linear (left) or circular (right) polarization states **(a)**. Active areas of channels (A and B) are formed between common and signal contacts. A band diagram under bias and a circuit diagram of each photodetector are shown on **(b)**. E_v, E_c and E_F are valence, conduction and Fermi energy levels respectively. Experimental setup used to obtain wavelength-dependent differential photocurrent measurements **(c)**.

As previously discussed, to permit a differential response two separate channels in each

photodetector are required. These channels should have a different response to the orthogonal polarization of the incident light. In this paper we present two photodetectors capable of distinguishing polarization states of either linearly or circularly polarised light (Fig.2). Each photodetector consists of three planar Al contacts twisted in a spiral (see Fig.1) to spatially match the circular beam profile used. Furthermore, the overall circular shape of the detector opens up the possibility of differentiating cylindrical vector beams[25] and other orthogonal beams. The width of the contacts and the spacing between them were chosen to be 1.25 µm and 1.5 µm respectively. The diameter of the photodetector is 50 µm. Each contact forms a Schottky barrier with the Si substrate. Taking the middle contact as common, the whole structure represents two metal-semiconductor-metal (MSM)[26] photodetectors connected back-to-back (see Fig.2b). Such a configuration can operate only under reverse bias. A schematic showing the double MSM photodetector band diagram under bias is shown on Fig.2b. The biasing of the photodiode's contacts leads to the presence of an electric field gradient in the semiconductor substrate. Every electron-hole pair generated by absorption in Si (in the case where $h\nu > E_g$) will be swept by this electric field to the electrodes, thus creating a photocurrent.

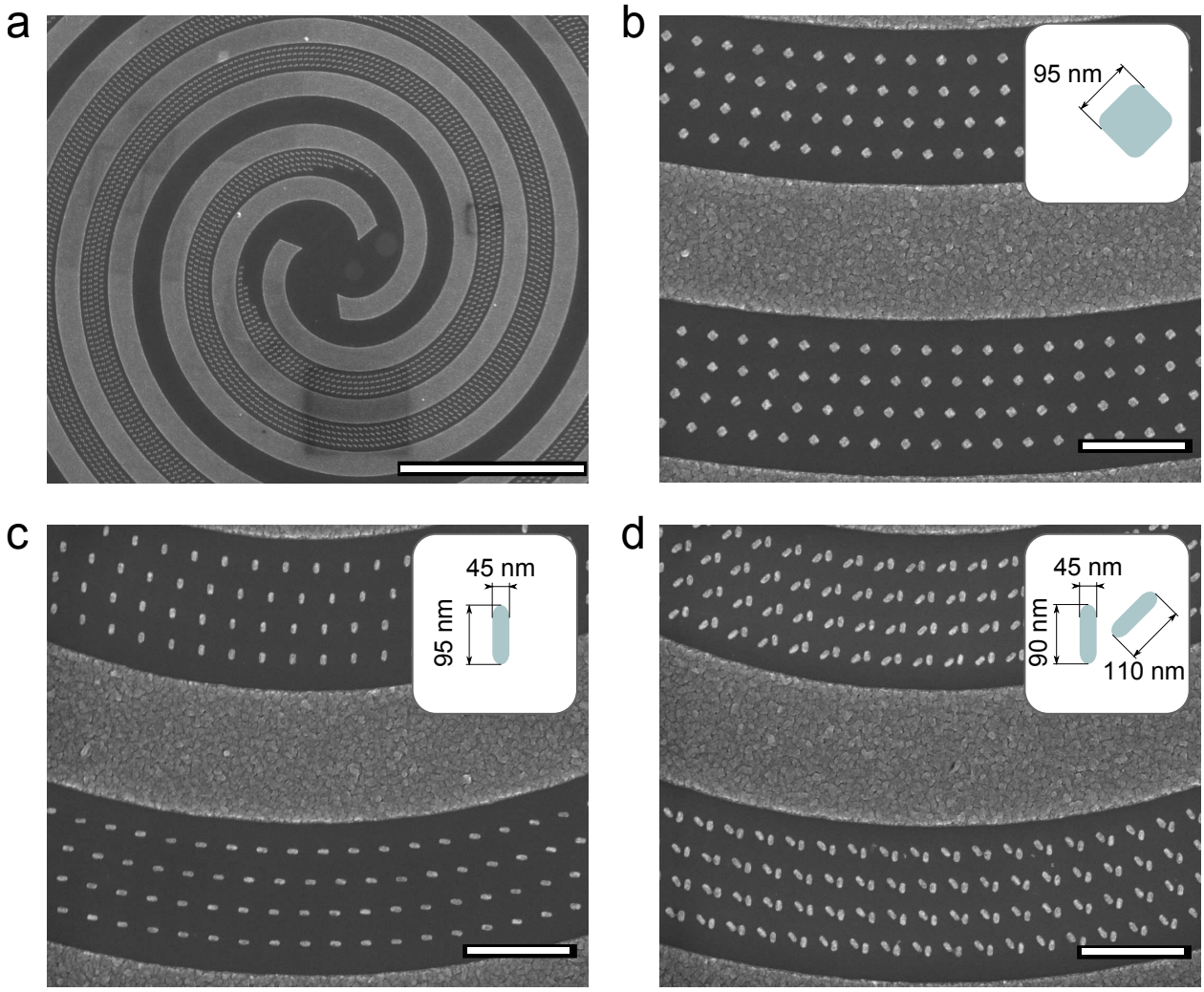

Figure 3: Scanning electron microscope image of the spiral photodetector **(a)**. Nanoantennas are absent between two signal contacts. The active regions with square **(b)**, rectangular **(c)** and chiral **(d)** nanoantennas respectively. The scale bar for image **(a)** is 10 µm and 1 µm for images **(b)**,**(c)**,**(d)**.

The photocurrent in each photodetector is determined by direct absorption of photons in their active regions. The number of photons transmitted into the Si and, hence, absorbed, is sensitive to the presence of nanoantennas on the surface and depends on their geometry. If the orientation of the antennas between each pair of contacts is different, there will be an imbalance between the photocurrents generated between each pair producing a polarization-dependent differential signal. The responsivity $R_q(\lambda)$ of each photodetector,[27] therefore, is affected by the spectral response[16] of the metasurface:

$$R_q(\lambda) = \eta_0 \frac{L}{L+W}(1 - e^{-\alpha(\lambda)d})S_q(\lambda) \tag{1}$$

where λ is the wavelength and q describes the polarization state of the incident field, $\alpha(\lambda)$ is an absorption coefficient of Si, d is the thickness of the MSM absorbing region, η_0 is a internal quantum efficiency, $S_q(\lambda)$ is the spectral response of the metasurface to polarization state q, L and W are the finger spacing and width respectively.

To tailor the sensitivity of each channel, nanoantennas were placed inside the photodetector's active regions (see Fig.3a). Each nanoantenna array responds to a different polarization state. In our design we used two different sets of nanoantennas. This produces a photodetector sensitive to orthogonal states of either linearly (Fig.3c) or circularly polarised light (Fig.3d). We also designed a photodetector with square nanoantennas (see Fig.3b) as a control.

The polarization sensitive metasurfaces consist of arrays of Al nanoantennas. We used single rectangular rods with a length of 95 nm and width of 45 nm to distinguish different states of linear polarization. We used a superposition of two 45 nm wide rods with lengths of 90 nm and 110 nm respectively to create a single layer chiral structure which responds differently to left and right circular polarization. These two rods were oriented at 45° to each other to maximise their chiral response.[24] To reinforce the role played by the nanoantenna geometry we also investigated a polarization insensitive control consisting of arrays of square nanoantennas of side 95 nm. We chose the spacing between these antennas to be 300 nm in both directions preventing near-field coupling. Nanoantennas and contacts were deposited in the same fabrication step (see methods) and all have a thickness of 85 nm.

Experimental results

The experimental setup is shown in Fig.2c. Half (HWP) and quarter (QWP) wave plates were used to control the linear and circular polarization states of the incident light to determine

the detector's responsivity. We performed a wavelength sweep from 500 nm to 800 nm with 25 nm step and 10 nm bandwidth. The photodetector was illuminated through a microscope objective with NA 0.4 to produce a spot matching the approximate size of the photodetector. The amplified photocurrent was recorded as a function of the rotation angle of the waveplates. A mean power of 2.5 µW (see Characterisation section for more information) and bias voltage of 3 V were maintained at each measurement during the experiment.

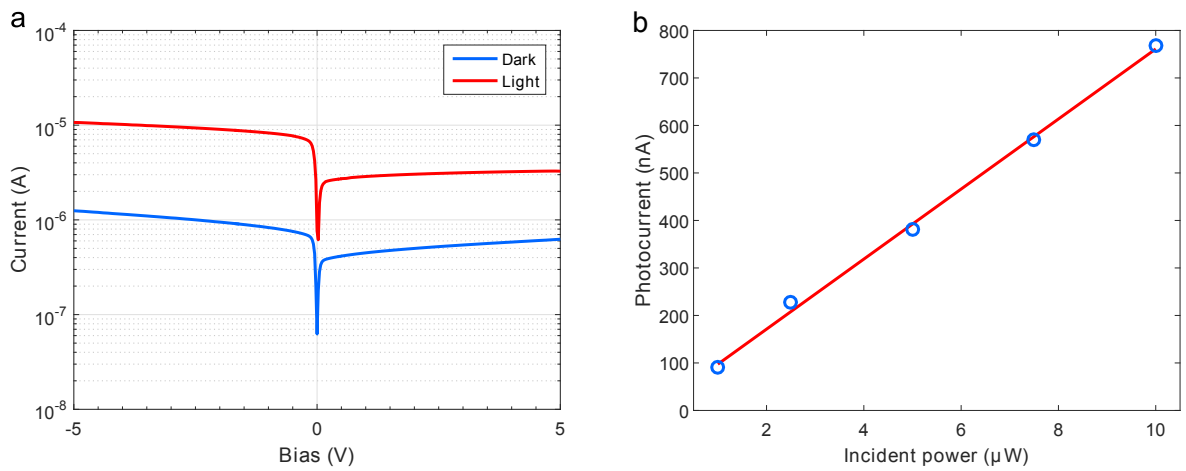

Figure 4: An IV characteristic showing the differential photodetector's channel in darkness and under illumination **(a)**. Generated photocurrent as a function of an incident power **(b)**.

An I-V characteristic of one arm of the differential photodetector with square nanoantennas is shown on Fig.4a. Since this detector consists of two back-to-back Schottky diodes, the characteristic has no forward bias region. A slight asymmetry of the curve for positive and negative bias can be explained by possible contamination of the surface during fabrication or defects introduced when bonding the sample into a chip carrier. The photocurrent generated by the photodetector as a function of the incident laser power at 625 nm wavelength and 3 V bias is shown on Fig.4b. Each channel of the photodetector was found to have a total responsivity of approximately 0.08 A/W.

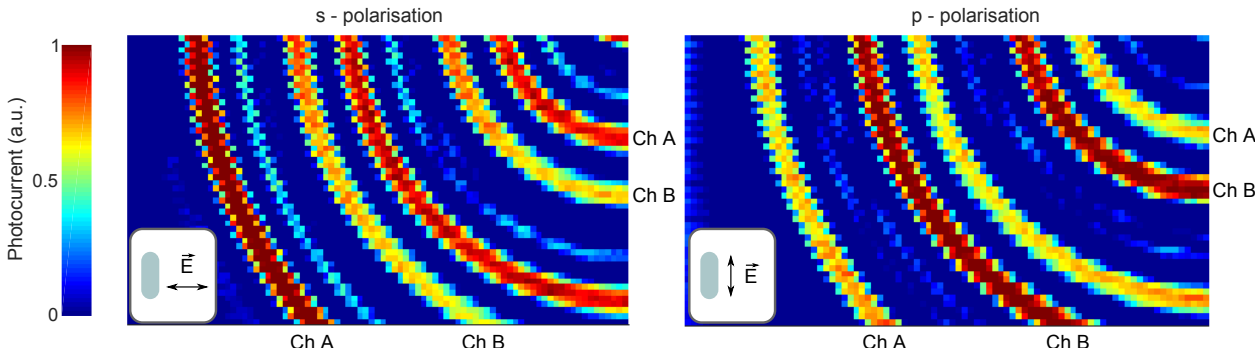

Figure 5: Normalised photocurrent maps of a photodetector with rectangular nanoantennas obtained with orthogonal polarization states of the light. The nanoantennas of channel A and B are oriented along x and y axis of the graph respectively. The maximum photocurrent appears when the incident electric field is perpendicular to the long axis of the nanoantenna.

To illustrate the principle of operation and demonstrate device performance we obtained photocurrent maps of a spiral differential photodetector with nanorod antennas (sensitive to linearly polarized light) using scanning photocurrent microscopy (SPCM).[28] The spatial position of the highly focused polarised beam was correlated with the photocurrent generated by each channel of the photodetector (Fig.5). These currents were then normalised and plotted together on the same scale. As can be seen in Fig.5 the photocurrent generation in each channel is different for each linear orthogonal polarization state. If the polarization of the incident light is parallel to the long axis of the nanorods (p polarization for Ch A) then there is a maximum in reflection from them resulting in lower photocurrent generation. This is in contrast to the hot electron generation regime when the photocurrent increases as a result of the higher absorption in nanoantennas.[16] Although this effect is also present in our device it is negligible due to the much lower efficiency compared with direct photon absorption in Si. The photocurrent generated outside the photodetector active area is much lower since for MSM photodetectors the maximum in the electric field gradient appears between the contacts. The light blue lines represent the increase of the photocurrent when the area near the metal contacts is illuminated with a focussed beam. Such behavior can be explained by electron-hole pair generation within the depletion region of each Schottky photodiode which has a width of less than 300 nm for the materials used.[29]

The normalised photocurrent at a wavelength of 625 nm produced by each photodetector integrated with either rectangular or chiral sets of nanoantennas is shown in Fig.6a,b,c as a function of HWP or QWP rotation angle respectively. Due to fabrication imperfections, each channel of the photodetector has a small variation in dark current. This results in a different offset of the output signal. For normalization purposes the dark current of each channel was subtracted from the output signals. A full rotation of a HWP takes 8 min during which the laser source exhibited significant intensity fluctuations (random changes in the output signal Fig.6a). The photocurrent from the detectors can also vary due to heating of the sample during measurements (a constant slope of the signal Fig.6b). These fluctuations are reflected in the raw signals (see Fig.6a,b,c) from both photodetectors. Although the average value of the signals from each photodetector individually varies, the differential photocurrent (see Fig.6d,e,f) has a relatively constant mean. Since the variation of power affects both photodetectors and remains in-phase, a simple subtraction of photocurrents eliminates the influence of this type of noise. An optical system utilizing differential spiral photodetectors, therefore, is relatively insensitive to fluctuations in signal intensity compared with conventional devices. This significantly increases a signal-to-noise ratio[30] and, therefore, opens up the possibility of higher communication speeds.

A nanorod antenna has a polarization response of a simple electric dipole oriented parallel to the long-axis of the rod. The maximum in its induced dipole moment appears when the electric field of the incident beam is directed parallel to the long axis of the rod (s and p polarized light, see Fig.6g). As can be seen from Fig.6d in the case of the array of rectangular nanoantennas the differential photocurrent follows Malus' law. At the same time, the difference between the two channels in the case of square nanoantennas (Fig.6e,i) remains zero for all polarization states. Such behavior can be explained by the absence of a polarization dependence in symmetric plasmonic nanoantennas.

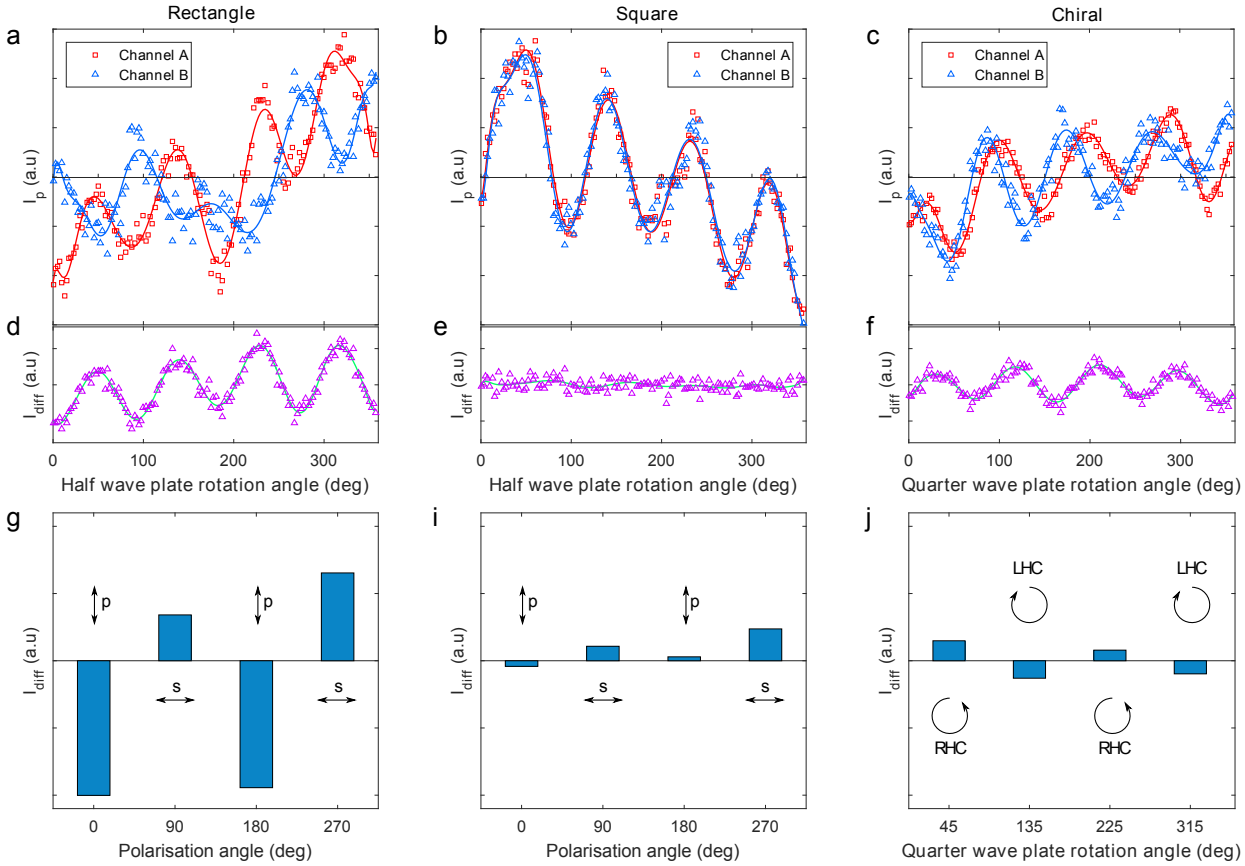

Figure 6: Normalised photocurrent affected by a signal power fluctuation from both channels of photodetectors with rectangular **(a)**, square **(b)** and chiral **(c)** sets of nanoantennas. As can be seen, differential photocurrent of each photodetector **(d)**,**(e)**,**(f)** is not affected by this type of noise. Figure **(g)**,**(i)** and **(j)** show the amplitude of the differential signal at each orthogonal state of polarization. The rotation of HWP and QWP are relative to the fast axis of the polariser.

In the case of the chiral metasurface (Fig.7f), the differential response is a result of two phenomena. The superposition of two rectangular nanoantennas oriented at 45° to each other has a net dipole moment which is rotated 22.5° counter- or clockwise (depending on the structure) relative to the longitudinal dimension of each rod. The rotation of a QWP changes the polarization of the beam from linear through elliptical to circular. In this case the effective linear component of the elliptical polarization state varies from -22.5° to 22.5°. The maximum difference of the photocurrent occurs when the effective linear polarization angle matches the net dipole moment of the chiral structure. At the same time the differential photocurrent changes for left and right circularly polarised light (see Fig.6j). As expected,

the chiral response is weaker compared to the linear due to the chiral dichroism for 2D structures used is around 10-15%.[24]

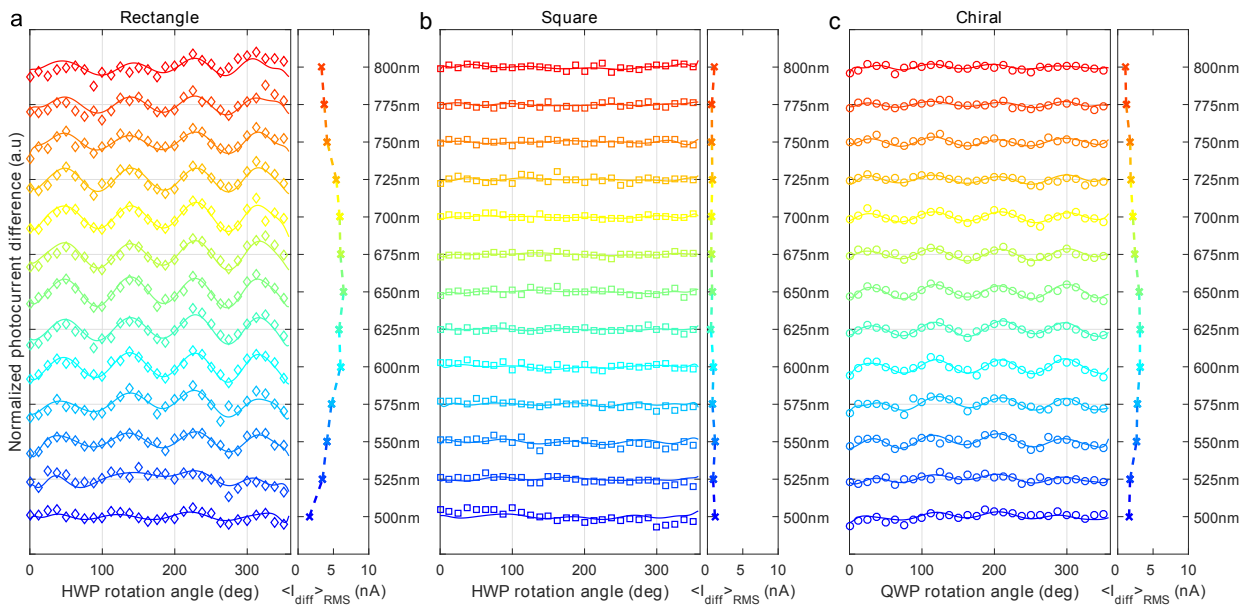

Figure 7: Differential signals at different wavelengths for photodetectors with rectangular **(a)**, square **(b)** and chiral **(c)** nanoantennas (the solid lines are polynomial fits of experimental data to guide the eye). The side graphs show root mean square values of photocurrent and reflect a differential responsivity at each wavelength.

The differential responses of photodetectors with rectangular, square and chiral nanoantennas for a range of wavelengths 500 nm - 800 nm is shown on Fig.7a,b,c. The insets in Fig.7 show root mean square values of photocurrent and reflect a differential responsivity at each wavelength. The use of Al as a material for the antennas leads to a relatively broad plasmonic resonance[31] compared with other metals such as silver and gold. Although in most applications this is an unwanted characteristic, in the case of polarization differential signaling it significantly reduces the sensitivity of the photodetector to signal wavelength drift and permits the use of the same design for each channel in wavelength division multiplexing systems. Operating at frequencies outside of the plasmonic resonance (below 575 nm) leads to a proportional decrease in metasurface polarization sensitivity. This fact explains the lower amplitude of the differential signal for short wavelengths. The decrease in amplitude at wavelengths above 750 nm can be explained by the decrease in absorption coefficient in

Si at these frequencies (see Eq.1).

Conclusion

We have demonstrated a compact, fully CMOS compatible plasmonic metasurface-enabled photodetector suitable for differential determination of orthogonal polarization states of light. Here we demonstrated the performance of two antenna designs suitable for the detection of states of either linear or circularly polarised light. Utilizing the spiral design presented here, the differential photodetector can potentially be applied, along with a suitable antenna design, to determining other polarization states of light, such as spatially modulated radially and azimuthally polarised optical beams.[32] The differential nature of the photodetector ensures that in-phase noise associated with changes in incident intensity, thermal or operating frequency fluctuations are strongly suppressed in the measured photocurrent difference. Substituting Si with a lower band gap semiconductor would open up the potential of producing a device that could operate at near-IR wavelengths. This photodetector design, therefore, could play a role in future telecommunication systems permitting increased operation speeds and even higher channel multiplexing densities due to improved signal-to-noise ratios. Furthermore, the concept presented here also lends itself to the development of devices for the full determination of the Stokes parameters of an incident field and, taking advantage of recent developments in the design of metasurfaces for sensing wavelength[33] and phase,[34] the concept could be extended to extraction of other information from optical fields.

Supporting Information Available

The Supporting Information is available free of charge on the ACS Publications website at DOI: 10.1021/acsphotonics.XXXXXXX.

- Additional information (10.1021/acsphotonics.XXXXXXX)

This material is available free of charge via the Internet at `http://pubs.acs.org/`.

Acknowledgements

This research was supported under the Australian Research Council's Discovery Projects funding scheme (project number DP110100221). This work was performed in part at the Melbourne Centre for Nanofabrication (MCN) in the Victorian Node of the Australian National Fabrication Facility (ANFF).

Methods

Simulations

Finite element method (FEM) analysis, implemented in COMSOL Multiphysics 5.1 with RF module, was used to simulate the resonance of different metasurfaces. Periodic boundary conditions in transverse and longitudinal directions were used in models to understand the effect of diffraction in case of array of nanoantennas. Scattering boundary condition below a 1 µm thick layer of Si terminated the model. The optical properties of Al used in the model were taken from experimental data for bulk material.[35]

Fabrication

Photodetectors were fabricated on low doped (bulk resistivity $\rho = 1 - 10$ Ω·cm) [100] n-type silicon wafer. Aluminium was used as a material for MSM contacts as well as nanoantennas. Such a choice of materials allows full compatibility with CMOS technology together with a low fabrication cost. The wafer was spincoated with 240 nm PMMA 950k resist and then exposed to create structures using a 100 kV EBPG5000+ electron beam lithography system. The pattern was developed in 1:3 MIBK:IPA solution for 1 minute. The native oxide layer on the silicon substrate was stripped using 4% hydrofluoric (HF) acid and immediately loaded

into IntlVac NanoChrome II e-beam evaporator. The aluminium layer with a thickness of 85 nm was deposited at 0.7Å/s. After evaporation a lift-off step in pure acetone was performed. During the lift-off process the solution was heated to 60 °C. A wet dicing saw (Disco DAD321) was used to separate the photodetectors for packaging in a ceramic PLCC20 package.

Characterisation

A Fianium SC450 supercontinuum white light source was used to characterise the samples. It was coupled with a Fianium SuperChrome VIS tunable filter to change a wavelength for measurements. A combination of polariser with half and quarter wave plates were used to produce and alter linear and circular polarization states respectively. HWP AHWP05M-600 and QWP AQWP05M-600 were fixed in a Thorlabs PRM1Z8 rotation stage. Utilisation of Nikon CFI Plan Fluor x20 long working distance objective permitted the uniformly illumination of the entire photodetector area. A polarization insensitive 50:50 beam splitter (Thorlabs BS013) was used to align the beam. After alignment it was withdrawn from the system. A pair of transimpedance amplifiers were designed and fabricated to work with the differential photodetector. The amplification coefficient was fixed on both channels and set to 10^6. A Keithley 487 source meter was used for precision biasing. The signal from the amplifiers was then sampled by a National Instruments USB-6343 DAQ. For SPCM measurements a Thorlabs S1FC635 fiber-coupled diode laser and Nikon CFI Plan Fluor x50 long working distance were used to obtain a spot size of 1 µm. The resolution in both x and y directions was of 200 nm.

Author contributions

EP and JJC conceived the concept, performed numerical simulations, fabricated the samples and contributed equally to this work. EP designed and fabricated specialised preamplifiers. EP and JJC conducted wavelength dependent differential responsivity measurements. EP performed scanning photocurrent measurements. TDJ and AR provided oversight of the

work. All authors discussed the obtained data and contributed to writing the manuscript.

References

(1) De Boer, J. F.; Milner, T. E.; van Gemert, M. J.; Nelson, J. S. Two-dimensional birefringence imaging in biological tissue by polarization-sensitive optical coherence tomography. *Opt. Lett.* **1997**, *22*, 934–936.

(2) Greenfield, N. J. Using circular dichroism spectra to estimate protein secondary structure. *Nat. Protoc.* **2006**, *1*, 2876–2890.

(3) Browne, D. E.; Rudolph, T. Resource-efficient linear optical quantum computation. *Phys. Rev. Lett.* **2005**, *95*, 010501.

(4) Koike-Tani, M.; Tani, T.; Mehta, S. B.; Verma, A.; Oldenbourg, R. Polarized light microscopy in reproductive and developmental biology. *Mol. Reprod. Dev.* **2015**, *82*, 548–562.

(5) Matharu, A. S.; Jeeva, S.; Ramanujam, P. Liquid crystals for holographic optical data storage. *Chem. Soc. Rev.* **2007**, *36*, 1868–1880.

(6) Zijlstra, P.; Chon, J. W.; Gu, M. Five-dimensional optical recording mediated by surface plasmons in gold nanorods. *Nature* **2009**, *459*, 410–413.

(7) Han, Y.; Li, G. Coherent optical communication using polarization multiple-input-multiple-output. *Opt. Express* **2005**, *13*, 7527–7534.

(8) Bozinovic, N.; Yue, Y.; Ren, Y.; Tur, M.; Kristensen, P.; Huang, H.; Willner, A. E.; Ramachandran, S. Terabit-scale orbital angular momentum mode division multiplexing in fibers. *Science* **2013**, *340*, 1545–1548.

(9) Javidi, B.; Nomura, T. Polarization encoding for optical security systems. *Opt. Eng.* **2000**, *39*, 2439–2443.

(10) Srituravanich, W.; Pan, L.; Wang, Y.; Sun, C.; Bogy, D. B.; Zhang, X. Flying plasmonic lens in the near field for high-speed nanolithography. *Nat. Nanotechnol.* **2008**, *3*, 733–737.

(11) Lin, L.; Goh, X. M.; McGuinness, L. P.; Roberts, A. Plasmonic lenses formed by two-dimensional nanometric cross-shaped aperture arrays for Fresnel-region focusing. *Nano Lett.* **2010**, *10*, 1936–1940.

(12) Yu, N.; Aieta, F.; Genevet, P.; Kats, M. A.; Gaburro, Z.; Capasso, F. A broadband, background-free quarter-wave plate based on plasmonic metasurfaces. *Nano Lett.* **2012**, *12*, 6328–6333.

(13) Drezet, A.; Genet, C.; Ebbesen, T. W. Miniature plasmonic wave plates. *Phys. Rev. Lett.* **2008**, *101*, 043902.

(14) Yokogawa, S.; Burgos, S. P.; Atwater, H. A. Plasmonic color filters for CMOS image sensor applications. *Nano Lett.* **2012**, *12*, 4349–4354.

(15) Li, W.; Coppens, Z. J.; Besteiro, L. V.; Wang, W.; Govorov, A. O.; Valentine, J. Circularly polarized light detection with hot electrons in chiral plasmonic metamaterials. *Nat. Commun.* **2015**, *6*.

(16) Knight, M. W.; Sobhani, H.; Nordlander, P.; Halas, N. J. Photodetection with active optical antennas. *Science* **2011**, *332*, 702–704.

(17) Tang, L.; Kocabas, S. E.; Latif, S.; Okyay, A. K.; Ly-Gagnon, D.-S.; Saraswat, K. C.; Miller, D. A. Nanometre-scale germanium photodetector enhanced by a near-infrared dipole antenna. *Nat. Photonics* **2008**, *2*, 226–229.

(18) Fischer, I. A.; Wu, J.-L.; Vogelgesang, R.; Schulze, J. Towards electrical detection of plasmons in all-silicon pin-diodes. *Phys. Status Solidi B* **2012**, *249*, 773–777.

(19) Anderson, D.; Dzatko, D. *Universal serial bus system architecture*; Addison-Wesley Longman Publishing Co., Inc., 2001.

(20) Eidson, S.; Gaines, B.; Wolf, P. 30.2: HDMI: High-Definition Multimedia Interface. Dig. Tech. Pap. - Soc. Inf. Disp. Int. Symp. 2003; pp 1024–1027.

(21) Joshi, A.; Wang, X.; Mohr, D.; Becker, D.; Wree, C. Balanced photoreceivers for analog and digital fiber optic communications. Defense and Security. 2005; pp 39–50.

(22) Liu, X.; Chandrasekhar, S.; Leven, A. Digital self-coherent detection. *Opt. Express* **2008**, *16*, 792–803.

(23) Maier, S. A. *Plasmonics: Fundamentals and Applications*; Springer, 2007.

(24) Eftekhari, F.; Davis, T. Strong chiral optical response from planar arrays of subwavelength metallic structures supporting surface plasmon resonances. *Phys. Rev. B* **2012**, *86*, 075428.

(25) Zhan, Q. Cylindrical vector beams: from mathematical concepts to applications. *Adv. Opt. Photonics* **2009**, *1*, 1–57.

(26) Berger, P. R. MSM photodiodes. *IEEE Potentials* **1996**, *15*, 25–29.

(27) Zimmermann, H. *Integrated silicon optoelectronics*; Springer, 2010.

(28) Allen, J. E.; Hemesath, E. R.; Lauhon, L. J. Scanning photocurrent microscopy analysis of Si nanowire field-effect transistors fabricated by surface etching of the channel. *Nano Lett.* **2009**, *9*, 1903–1908.

(29) Sharma, B. *Metal-semiconductor Schottky barrier junctions and their applications*; Springer Science & Business Media, 2013.

(30) Sklar, B. *Digital Communications*; Prentice Hall NJ, 2001; Vol. 2.

(31) Knight, M. W.; King, N. S.; Liu, L.; Everitt, H. O.; Nordlander, P.; Halas, N. J. Aluminum for plasmonics. *ACS Nano* **2013**, *8*, 834–840.

(32) Ren, H.; Li, X.; Zhang, Q.; Gu, M. On-chip noninterference angular momentum multiplexing of broadband light. *Science* **2016**, aaf1112.

(33) Tan, S. J.; Zhang, L.; Zhu, D.; Goh, X. M.; Wang, Y. M.; Kumar, K.; Qiu, C.-W.; Yang, J. K. Plasmonic color palettes for photorealistic printing with aluminum nanostructures. *Nano Lett.* **2014**, *14*, 4023–4029.

(34) Davis, T. J.; Gómez, D. E.; Eftekhari, F. All-optical modulation and switching by a metamaterial of plasmonic circuits. *Opt. Lett.* **2014**, *39*, 4938–4941.

(35) Johnson, P. B.; Christy, R.-W. Optical constants of the noble metals. *Phys. Rev. B* **1972**, *6*, 4370.

Graphical TOC Entry